Determination of defect distributions from admittance measurements and application to Cu(In,Ga)Se_2 based heterojunctions

T. Walter, R. Herberholz,[a] C. Müller, and H. W. Schock
Institut für Physikalische Elektronik, Universität Stuttgart, Pfaffenwaldring 47, D-70569 Stuttgart, Germany

(Received 2 January 1996; accepted for publication 9 July 1996)

A method to deduce energy distributions of defects in the band gap of a semiconductor by measuring the complex admittance of a junction is proposed. It consists of calculating the derivative of the junction capacitance with respect to the angular frequency of the ac signal corrected by a factor taking into account the band bending and the drop of the ac signal over the space charge region of the junction. Numerical modeling demonstrates that defect distributions in energy can be reconstructed by this method with high accuracy. Defect distributions of polycrystalline Cu(In,Ga)Se_2 thin films are determined by this method from temperature dependent admittance measurements on heterojunctions of Cu(In,Ga)Se_2 with ZnO that are used as efficient thin film solar cells. © *1996 American Institute of Physics.* [S0021-8979(96)03920-5]

I. INTRODUCTION

Defect levels in the band gap of semiconductors often give rise to an anomalous behavior of the material. This is especially so for amorphous and polycrystalline semiconductors which play an important role for photovoltaics, sensors, varistors, and other thin film applications and exhibit properties that require advanced characterization techniques and interpretations. For monocrystalline semiconductors measurement techniques such as deep level transient spectroscopy (DLTS)[1] and photoluminescence (PL) have been proposed and applied in order to identify discrete defects in the band gap. However, in the case of amorphous semiconductors, e.g., *a*-Si:H, a continuous energy distribution of defects that prohibits a straightforward interpretation of these measurements exists. Therefore several techniques such as modulated photocurrent (MPC),[2] photoconductivity (PC),[3] time of flight (TOF),[4] and deep-level transient spectroscopy (DLTS)[5] have been developed or extended successfully to identify these defect distributions. Recently, similar distributions of defects were identified in polycrystalline $CuInSe_2$,[6,7] which plays an important role in thin film photovoltaics.[8] A continuous energy distribution of defects has also been detected at grain boundaries of multicrystalline Si.[9]

In this article we propose a method for the determination of energy defect distributions from frequency-dependent junction capacitance measurements. Admittance spectroscopy has been proposed as a tool for the identification of discrete traps in the band gap of a semiconductor[10–16] or to study interface states in metal–oxide–semiconductor (MIS) and Schottky junctions.[17] Modeling of the capacitance has been carried out with respect to a continuous distribution of states.[18] Also, a method to improve the resolution of admittance spectroscopy by a Tikhonov regularization has been proposed.[19] The extraction of the slope of $1/C(V)^2$ plots at different angular frequencies of the ac signal in capacitance–voltage ($C-V$) measurement has been used to gain information about the density of states in *a*-Si Schottky barriers.[20,21] However, no method has been suggested that allows a simple evaluation of the frequency dependence of the junction capacitance for a broad distribution of defects.

From first principle rate equations, which determine the occupation of a defect, a theory for the frequency dependence of the junction capacitance for a distribution of defects will be developed. On the basis of these calculations a method for the extraction of defect distributions from admittance data will be proposed. In order to demonstrate the capability (and limitations) of this method, capacitance data have been modeled for nip and n^+p junctions with different distributions of traps in energy. From this calculated admittance, the density of states has been extracted and compared to the original defect distribution used as input data. In a second step measurements on ZnO/Cu(In,Ga)Se_2-based heterojunctions, which are used as efficient thin film solar cells, are presented.

This article is divided into two main parts. In the first part a theory is developed and discussed. The application of this theory should be of general interest for the investigation of defects in semiconductors distributed in energy. Thus, this part should be of interest for the general reader, whereas in the second part specific results on chalcopyrite based heterojunctions are presented. These are discussed separately, demonstrating the application of the procedure developed in the first part and giving insight into the defects controlling the electronic properties in these thin film solar cells.

II. THEORY

A theory for the determination of an energy distribution of defects from junction admittance data will be developed along the following guidelines:

(1) contribution of a defect in the band gap to the junction admittance from first principle rate equations;

(2) effectiveness of this contribution to the junction capacitance with respect to the energy position of this defect in the band gap;

(3) integration of the contribution of single defects in energy and space; and

(4) influence of the junction type.

[a]Electronic mail: rainer@ipers1.e-technik.uni-stuttgart.de

A. Occupation of defects and its contribution to the junction admittance

A change in the electron occupation of a defect in the band gap at an energy E is accomplished by the capture of electrons and holes characterized by their capture coefficients $\beta_{n,p}$ and by the reemission of holes and electrons which additionally depends on the depth of the defect

$$\frac{dn_t}{dt} = \beta_n n(N_t - n_t) - \beta_p p n_t - \beta_n N_c n_t e^{-[(E_c - E)/kT]} + \beta_p N_v (N_t - n_t) e^{-[(E - E_v)/kT]}. \quad (1)$$

N_t denotes the density of the defect, n_t the density of defects occupied with an electron, p,n the free carrier densities, and $N_{v,c}$ the effective density of states in the valence or conduction band, respectively.

For a small ac signal applied to the junction all carrier densities and the occupation of the defects are composed of a steady state value and an ac component:

$$n = n^{=} + \tilde{n} e^{i\omega t}, \quad p = p^{=} + \tilde{p} e^{i\omega t}, \quad n_t = n_t^{=} + \tilde{n}_t e^{i\omega t}, \quad (2)$$

with

$$\frac{dn_t}{dt} = i\omega \tilde{n}_t e^{i\omega t}, \quad (3)$$

where ω is the angular frequency of the ac signal.

Thus Eq. (1) can be rewritten as

$$\begin{aligned} i\omega \tilde{n}_t e^{i\omega t} = {} & \beta_n (n^{=} + \tilde{n} e^{i\omega t})(N_t - n_t^{=} - \tilde{n}_t e^{i\omega t}) \\ & - \beta_p (p^{=} + \tilde{p} e^{i\omega t})(n_t^{=} + \tilde{n}_t e^{i\omega t}) \\ & - \beta_n N_c (n_t^{=} + \tilde{n}_t e^{i\omega t}) e^{-[(E_c - E)/kT]} \\ & + \beta_p N_v (N_t - n_t^{=} - \tilde{n}_t e^{i\omega t}) e^{-[(E - E_v)/kT]}. \end{aligned} \quad (4)$$

The steady state condition of Eq. (1) has to be fulfilled in Eq. (4), i.e.,

$$0 = \beta_n n^{=} (N_t - n_t^{=}) - \beta_p p^{=} n_t^{=} - \beta_n N_c n_t^{=} e^{-[(E_c - E)/kT]} + \beta_p N_v (N_t - n_t^{=}) e^{-[(E - E_v)/kT]}. \quad (5)$$

Neglecting products of ac components, using (5) and the fact that the equilibrium occupation of a defect at an energy E, i.e., for a zero biased junction, is determined by the Fermi function $f_n(E)$, the ac component of the occupation of a defect can be deduced from (4):

$$\tilde{n}_t = \frac{1}{i\omega + \omega_0} [\beta_n \tilde{n} - f_n(E)(\beta_n \tilde{n} + \beta_p \tilde{p})] N_t, \quad (6)$$

where ω_0 stands for

$$\omega_0 = \beta_n n^{=} (1 + e^{-[(E_f - E)/kT]}) + \beta_p p^{=} (1 + e^{-[(E - E_f)/kT]}), \quad (7)$$

since

$$N_c e^{-[(E_c - E)/kT]} = n^{=} e^{-[(E_f - E)/kT]}; \qquad N_v e^{-[(E - E_v)/kT]} = p^{=} e^{-[(E - E_f)/kT]}. \quad (8)$$

This analysis can be easily extended to an applied dc bias by extracting the occupation of a defect ($n_t^{=}$) from (5) instead of using the Fermi function.

The current into such a defect consists of a hole and of an electron current, both with a dc and an ac component. In order to find the correct polarity of the different contributions one has to consider the situation in a pn junction. When a positive bias is applied to the junction, electrons from the n-type semiconductor and holes from the p-type semiconductor are injected into the space charge region and captured/reemitted in/from defects. Therefore, both the capture of electrons and holes has to be counted as positive current. Taking into account these considerations for the polarity of the currents, the rate equations for the capture and reemission of carriers into/from defects lead to the following expression for the current which is similar to expression (1):

$$\begin{aligned} j = j^{=} + \tilde{j} = q(\beta_n n(N_t - n_t) + \beta_p p n_t \\ - \beta_n n_t n^{=} e^{-[(E_f - E)/kT]} \\ - \beta_p (N_t - n_t) p^{=} e^{-[(E - E_f)/kT]}). \end{aligned} \quad (9)$$

Using the same ac small signal approach as above, the admittance of a junction due to a defect in the band gap can be deduced from (9). The capacitance due to the charging and discharging of a defect in addition to the depletion layer capacitance is then the imaginary part of (9) divided by the external ac signal and by the angular frequency. The analysis of (9) is simplified by the fact that only $\tilde{n}_t$ possesses an imaginary part. $\tilde{n}$ and $\tilde{p}$, i.e. the ac components of the carrier densities in the bands, are in phase with the applied ac signal and thus possess no imaginary part. Therefore, only terms containing $\tilde{n}_t$ have to be considered:

$$C' = \frac{im(\tilde{j})}{\omega \tilde{u}_{\text{ext}}} = \frac{q\, im(\tilde{n}_t)}{\omega \tilde{u}_{\text{ext}}} [\beta_p p^{=} (1 + e^{-[(E - E_f)/kT]}) - \beta_n n^{=} (1 + e^{-[(E_f - E)/kT]})]. \quad (10)$$

With

$$\omega_1 = \beta_p p^{=} (1 + e^{-[(E - E_f)/kT]}) - \beta_n n^{=} (1 + e^{-[(E_f - E)/kT]}), \quad (11)$$

and using Eq. (6), Eq. (10) can be written as

$$C' = \frac{q}{\tilde{u}_{\text{ext}}} \frac{\omega_1}{\omega^2 + \omega_0^2} [-\beta_n \tilde{n} + f_n(E)(\beta_n \tilde{n} + \beta_p \tilde{p})] N_t. \quad (12)$$

The dependence of (12) on the angular frequency ω can be understood readily. For $\omega \ll \omega_0$ the occupation of the defect can follow the applied ac signal and the charging and discharging of the defect contribute to the capacitance, whereas for high modulation frequencies the defects cannot follow and no contribution to the capacitance arises. $\omega = \omega_0$ can be considered as a limit for which a defect can be charged and discharged by the ac modulation. The same information is contained in the conductance which is the real part of (9) divided by the external ac bias. We restrict our analysis to the capacitance, keeping in mind that the same information can be obtained from conductance measurements.

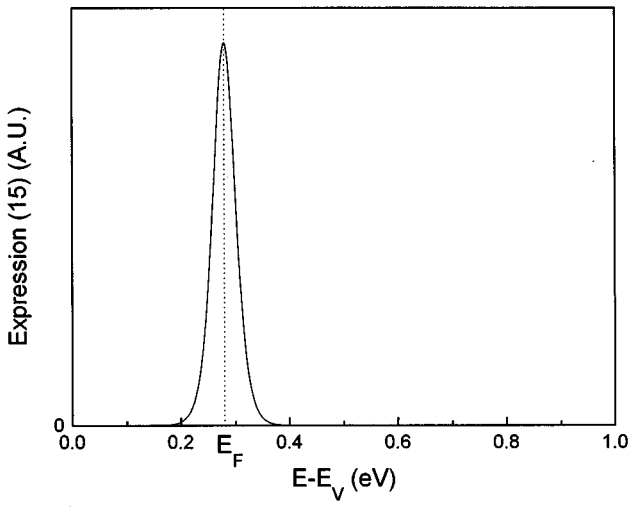

FIG. 1. Effectiveness of the contribution of a defect to the junction capacitance with respect to the energy depth.

In a *pn* junction the contribution of a single defect to the capacitance as described by (12) has to be integrated in energy and space.

B. Effectiveness of defects for the junction admittance

In order to obtain an analytical solution, a simple *nip* junction as sketched in Fig. 2(a) with a constant field region (width w) will be considered and will be discussed later in the article. As a first step the contribution of an energy distribution of defects $N_t(E)$ at a certain position in the depletion region to the capacitance (C') will be evaluated. The free carrier densities are determined by the position of the Fermi level. It is assumed that $p^{=} \gg n^{=}$, i.e., the Fermi level is closer to the valence band. The case $n^{=} \gg p^{=}$ can be treated in an analogous way. Furthermore, the angular frequency is slow enough, so that all traps can follow the ac signal, i.e., $\omega \ll \omega_0$. In a small signal approach the ac components of the carrier densities can be written as

$$\tilde{p} = p^{=} \frac{q\tilde{u}_p}{kT}; \quad \tilde{n} = n^{=} \frac{q\tilde{u}_n}{kT}. \tag{13}$$

Here, $q\tilde{u}_{n,p}$ stands for the local shift of the quasi-Fermi levels with respect to the band edges when applying an ac signal to the junction. Thus, (12) can be written for $\omega \ll \omega_0$ as

$$C' = \frac{q^2}{kT} \frac{1}{\tilde{u}_{\text{ext}}} \frac{\omega_1}{\omega_0^2} [-\beta_n n^{=} \tilde{u}_n + f_n(E)(\beta_n n^{=} \tilde{u}_n + \beta_p p^{=} \tilde{u}_p)] N_t(E). \tag{14}$$

Due to the energy dependence of ω_1, ω_0, and f_n not all defects in the band gap contribute with the same efficiency to the capacitance. The function

$$\frac{\omega_1}{\omega_0^2} [\beta_n n^{=} - f_n(E)(\beta_n n^{=} + \beta_p p^{=})] \tag{15}$$

preponderates the contribution of defects $N_t(E)$ with respect to the energy position in the band gap. Expression (15) is plotted versus the distance from the valence band in Fig. 1, assuming $E_f - E_v = 280$ meV, i.e., $p^{=} \gg n^{=}$. From Fig. 1 it is obvious that expression (15) samples the defect distribution $N_t(E)$ around the Fermi level.

In the vicinity of the Fermi level, (14) can be expressed as ($p^{=} \gg n^{=}$):

$$C'(E) = \frac{q^2}{kT} \frac{\tilde{u}_p}{\tilde{u}_{\text{ext}}} \frac{1}{2 + e^{-[(E-E_f)/kT]} + e^{-[(E_f-E)/kT]}} N_t(E). \tag{16}$$

For an energy distribution of defects, (16) has to be integrated in energy. Due to the fact that (16) decreases exponentially with increasing distance from the Fermi level, the integration limits can be extended to $\pm\infty$:

$$C'' = \frac{q^2}{kT} \frac{\tilde{u}_p}{\tilde{u}_{\text{ext}}} \int_{-\infty}^{\infty} \frac{1}{2 + e^{-[(E-E_f)/kT]} + e^{-[(E_f-E)/kT]}} N_t(E) dE. \tag{17}$$

Under the assumption that $N_t(E)$ is constant around $E = E_f$ (the validity of which will be discussed below), (17) can be integrated analytically, leading to a simple result

$$C'' = q^2 \frac{\tilde{u}_p}{\tilde{u}_{\text{ext}}} N_t(E_F). \tag{18}$$

These relations can be interpreted in the following way. For a continuous energy distribution of defects in the band gap, only the defects at the Fermi level efficiently contribute to the capacitance if the angular frequency is low enough and the value of the capacitance is given by (18).

$N_t(E)$ was assumed to be constant around E_f. In order to estimate the width of the sampling function, (16) can be developed around E_f. The intersects of this function with the energy axis are $E_f \pm 2kT$. Therefore, if $N_t(E)$ can be considered as constant from $E_f - 2kT$ to $E_f + 2kT$, (18) is valid.

It should be mentioned that for $n^{=} \gg p^{=}$ the same expression for the capacitance (and the same polarity) is obtained (with $\tilde{u}_n$ instead of $\tilde{u}_p$). Only for $p^{=} = n^{=}$ and $E = E_f$ does no contribution to the junction capacitance arise (assuming equal capture cross sections for electrons and holes). This can be understood in terms of efficient recombination which occurs in a *pn* junction in the vicinity of $p = n$ for defects between the quasi-Fermi levels. In this case holes and electrons are equally captured in the defects, not changing the occupation of the defect but leading to a recombination current. If an ac signal is applied to the junction at zero bias, recombination is most efficient where the Fermi level crosses the midgap position. Figure 2 shows the band diagram of a *nip* junction [Fig. 2(a)], and the corresponding dependences of $n^{=}, p^{=}$ [Fig. 2(c)], and $\tilde{u}_n, \tilde{u}_p$ [Fig. 2(b)]. In Fig. 2(d) the preponderant function (15) is shown for the *nip* junction of Fig. 2(a) taking into account the position dependence of $\tilde{u}_p, \tilde{u}_n$ as illustrated in Fig. 2(b). Figure 2(d) illustrates the sampling character of (15) at $E = E_f$, the fact that no contribution to the capacitance arises for $p = n$ and the restriction that only defects in the space charge region contribute to the junction capacitance.

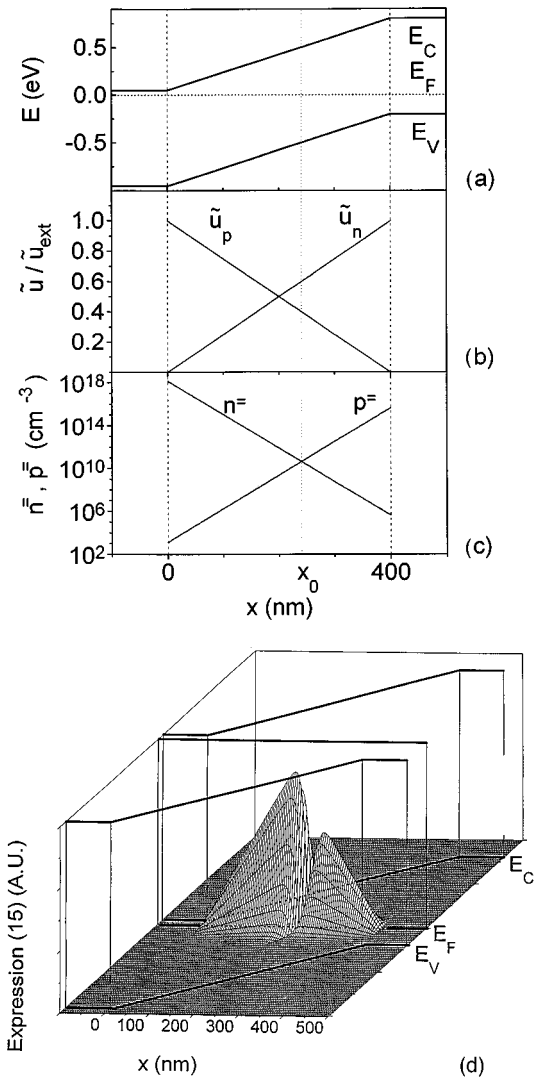

FIG. 2. An *nip*-junction: (a) band diagram; (b) $\tilde{n}_n, \tilde{u}_p$; (c) $n^=, p^=$. (d) Effectiveness of the contribution of a defect to the junction capacitance.

C. Contribution of defects in a junction to the admittance

In a second step the integration in space has to be carried out. Additionally one has to take into account that at a certain angular frequency not all defects can follow and contribute to the junction capacitance. Integration of the contributions to the capacitance in space for defects at the Fermi level also means integration in energy as the distance of the Fermi level to the band edges depends on the position in the junction. The sampling of $N_t(E)$ at E_f implies a relation between the position in the depletion region (*i* layer) and the depth in which defects effectively contribute. The relation between the position of the Fermi level in the junction and the energy position in the band gap with respect to the valence band for the junction of Fig. 2(a) (*nip* junction) is given by

$$E = E_f = E_{fn\infty} - \frac{x}{w} qU_d, \tag{19}$$

where U_d denotes the built-in voltage in the junction, w is the width of the intrinsic layer, and $E_{fn\infty}$ the energy position of the Fermi level with respect to the valence band edge in the *n*-type semiconductor.

In this analysis we will restrict ourselves to defects between the midgap position and the position of the Fermi level. Thus the lower limit of the integration of the capacitance with respect to Fig. 2(a) is $x = x_0$, i.e., the part of the junction for which $p^= \gg n^=$ is valid. The upper limit of the integration is determined by the fact that outside the depletion region only the electron density, i.e., the density of the minorities, is modulated. However, inside the depletion region the modulation of holes by far exceeds the modulation of the electron density outside the depletion region (*i* layer), thus, restricting the region where defects efficiently contribute to the depletion region (*i* layer) as demonstrated in Fig. 2(d). Therefore, the upper limit for the integration is the boundary of the depletion region. For a slow enough angular frequency, all defects between the midgap position and the Fermi level in the bulk of the *p*-type semiconductor contribute to the capacitance. If not all defects can follow, only defects between a certain ''demarcation energy'' and the Fermi level in the bulk of the *p*-type semiconductor contribute to the capacitance. This demarcation energy can be calculated with (7) from $\omega = \omega_0$ representing the maximum frequency for which a defect at an energy E_ω with respect to the valence band according to (12) can be charged and discharged by the ac signal and therefore contributes to the junction capacitance

$$\omega = \omega_0 = 2\beta_p N_v e^{-(E_\omega/kT)}; \quad E_\omega = kT \ln \frac{2\beta_p N_v}{\omega}. \tag{20}$$

Therefore the integral in space runs from a certain x_1, where the Fermi energy and E_ω cross, to the boundary of the depletion region or, in terms of energy from E_ω to $E_{fp\infty}$,

$$C = \frac{q^2}{\tilde{u}_{\text{ext}}} \int_{x_1}^{w} \tilde{u}_p(x) N_t(E_f(x)) dx$$

$$= -\frac{q^2}{\tilde{u}_{\text{ext}}} \int_{E_\omega}^{E_{fp\infty}} \tilde{u}_p(x(E)) N_t(E) \frac{w}{qU_d} dE, \tag{21}$$

where $E_{fp\infty}$ represents the position of the Fermi level in the bulk of the *p*-type semiconductor. In order to evaluate the defect distribution from the dependence of the capacitance on the angular frequency the following operation has to be carried out:

$$\frac{dC}{d\omega} = \frac{dC}{dE_\omega} \frac{dE_\omega}{d\omega}$$

with

$$\frac{dE_\omega}{d\omega} = -\frac{kT}{\omega}. \tag{22}$$

Assuming $\tilde{u}_p = \text{const.} = \tilde{u}_{\text{ext}}$ the defect distribution can be evaluated using (21) and (22),

$$N_t(E_\omega) = -\frac{U_d}{qw} \frac{dC}{d\omega} \frac{\omega}{kT}. \tag{23}$$

Thus, under these assumptions the defect distribution at an energy E_ω can be determined by calculating the derivative in a $C(\omega)$ measurement.

A better approximation can be obtained by taking into account the position dependence of $\tilde{u}_p$. Now $\tilde{u}_p$ is the shift of the valence band with respect to the hole quasi-Fermi level as a consequence of an applied ac signal and is therefore related to the drop of the applied bias over the depletion region. At $x=w$ the valence band is fixed with respect to the Fermi level. As for a nip junction, a linear drop of the applied bias over the depletion region occurs, $\tilde{u}_p$ increases linearly from $x=w$ to $x=0$ reaching the value of the externally applied signal $\tilde{u}_{\text{ext}}$ at $x=0$

$$\tilde{u}_p=\tilde{u}_{\text{ext}}\frac{w-x}{w}. \tag{24}$$

Taking (24) into account, (23) has to be modified using (19)

$$N_t(E_\omega)=-\frac{U_d^2}{w[qU_d-(E_{fn\infty}-E_\omega)]}\frac{dC}{d\omega}\frac{\omega}{kT}. \tag{25}$$

For a parabolic band that represents the situation in a n^+p junction, the density of states can be evaluated in a similar way taking into account the position dependences of $\tilde{u}_{n,p}$ and the relation between the distance of the Fermi level from the valence band and the position in the junction:

$$N_t(E_\omega)=-\frac{2U_d^{3/2}}{w\sqrt{q}\sqrt{qU_d-(E_g-E_\omega)}}\frac{dC}{d\omega}\frac{\omega}{kT}. \tag{26}$$

III. MODELING OF THE JUNCTION CAPACITANCE AND DETERMINATION OF DEFECT DISTRIBUTIONS

In order to test the method developed above with respect to the evaluation of the defect distribution from admittance data, the contribution of a defect distribution to the capacitance was calculated by integration of (12) in energy and in space for an n^+ip and an n^+p junction, both with a band gap of 1 eV. The thickness of the i layer in the n^+ip junction and the width of the space charge region of the n^+p junction were both 400 nm with a energy distance of the Fermi level in the bulk of the p-type semiconductor to the valence band of 200 meV. A degenerate n-type semiconductor was assumed. Two types of defect distributions and a superposition of both were considered.

A Gaussian type of defect:

$$N_t(E)=N_g e^{-[(E_t-E)^2/\sigma^2]}. \tag{27}$$

A tail-like distribution of defects:

$$N_t(E)=N_e e^{-[(E-E_v)/kT^*]}. \tag{28}$$

The capacitance data as obtained from numerical integration in energy and space are shown in Fig. 3(a) for an n^+ip and an n^+p junction. The frequency dependence of the Gaussian type of defect distribution exhibits a rather pronounced step, whereas for the tail-like distribution this step is less steep due to the broader distribution of defects.

From this data the density of states according to (25) and (26) was calculated. The results for the two types of junctions, together with the input data, are presented in Figs. 3(b) and 3(c). The input density of states is reproduced well by the approximation suggested above. For the tail-like distribution input and output data differ for energies shallower than about 200 meV and deeper than about 450 meV. The deviation for shallow states is due to the fact that only states deeper than the Fermi level in the bulk of the p-type material can be detected. Furthermore, states at the midgap position predominantly act as recombination centers (for equal capture cross sections of electrons and holes) and can therefore not be detected by capacitance measurements. This procedure of calculating the admittance and determining the density of states from the admittance data was performed on

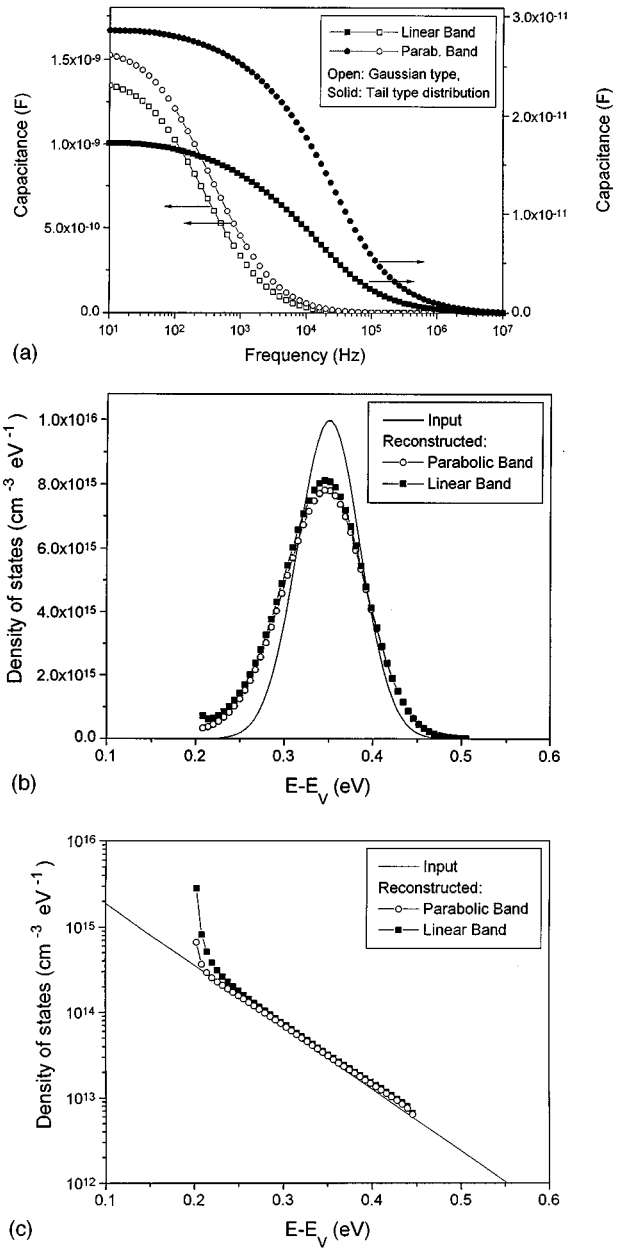

FIG. 3. (a) Calculated $C(\omega)$ for a Gaussian type and tail-like defect distribution (linear and parabolic band). (b) Input and reconstructed defect distribution for the Gaussian type defect distribution. (c) Input and reconstructed defect distribution for the tail-like defect distribution.

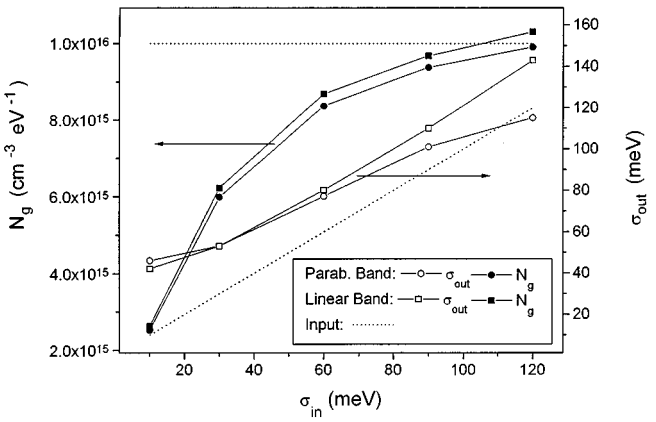

FIG. 4. Width and magnitude [N_g (input)$=10^{16}$ cm^{-3} eV^{-1}] of the Gaussian type of defect distribution: comparison of input and reconstruction.

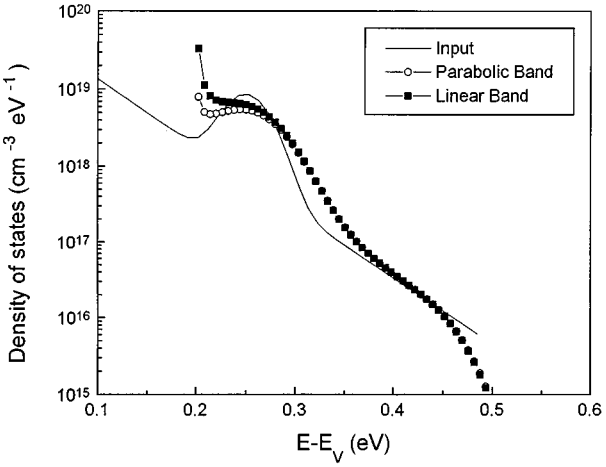

FIG. 6. Input and reconstructed defect distribution for a superposition of Gaussian type and tail-like defects.

Gaussian peaks with varying width (σ) and with tail-like distributions with different slopes (kT^*). For a Gaussian defect distribution the width (σ_{out}) of the defect distribution as deduced from the calculated admittance data is shown as a function of the width of the input data (σ_{in}) in Fig. 4 for the two types of junctions. For a narrow Gaussian defect as input a significant broadening occurs in the reconstructed data. This is partly due to a severe violation of the condition that the density of defects has to be constant within $\pm 2kT$ at the Fermi level, which is certainly not the case for such a narrow distribution of defects. Apart from this deviation the input data is accurately reproduced by the procedure suggested above. Additionally the values of the reproduced maximum of the density of states are shown for the Gaussian defects with different widths for an input value of 10^{16}/cm^3 eV (N_g) in Fig. 4. In Fig. 5 the slopes of tail-like distributions and the corresponding N_e values are compared for input and reconstructed data.

In Fig. 6 a more complex distribution of defects consisting of a Gaussian defect superimposed on a valence band tail is considered. The comparison of output and input data clearly demonstrates that this evaluation procedure reproduces the input distribution of defects with good accuracy. However, this is only valid for defects at the valence band between the Fermi level in the bulk and the midgap position. If defects extend into the upper half of the band gap, admittance spectroscopy cannot distinguish between states close to the valence band and states close to the conduction band. This is illustrated for the defect distribution of Fig. 7 consisting of two Gaussian defects superimposed on a conduction band tail and a valence band tail. The distribution of defects as deduced from capacitance data is also plotted in Fig. 7. Due to the fact that this method cannot distinguish between conduction band and valence band states two Gaussian peaks appear superimposed on the valence band tail which does not reproduce the input data. From an experimental point of view additional measurements such as DLTS or bias dependent admittance measurements should be carried out in order to clearly identify if a hole or electron trap is present.

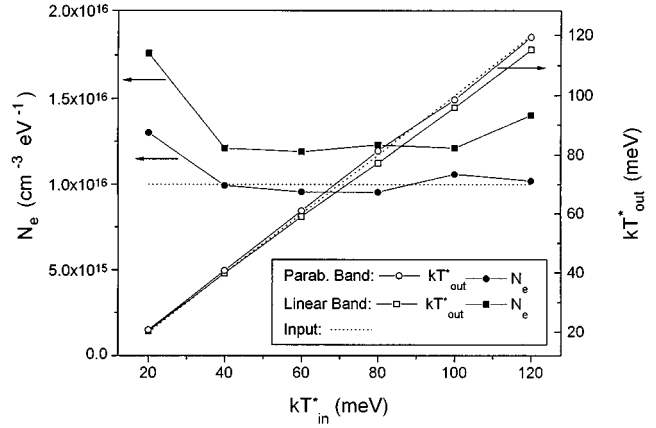

FIG. 5. Slopes and magnitude [N_e (input)$=10^{16}$ cm^{-3} eV^{-1}] of tail-like defect distribution: comparison of input and reconstruction.

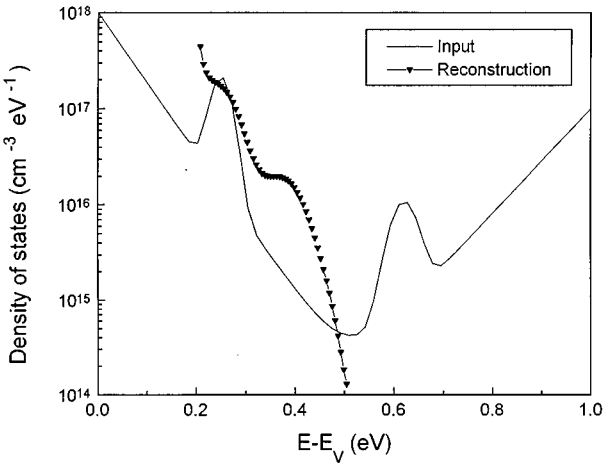

FIG. 7. Input and reconstructed defect distribution for valence band and conduction band states.

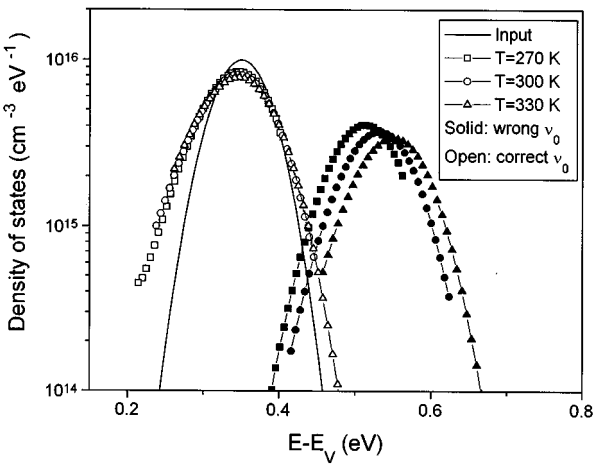

FIG. 8. Input and reconstructed defect distribution for different temperatures using the ''correct,'' i.e., input, and the ''wrong'' attempt-to-escape frequency. The wrong attempt to escape frequency differs by three orders of magnitude from the input value.

IV. DISCUSSION

A simple method to obtain the energy distribution of defects from admittance measurements was proposed. This evaluation scheme consists of calculating the derivative of the frequency dependence of the capacitance accompanied by scaling the frequency into an energy axis. Assuming a angular frequency range from 10^2 to 10^6 Hz [in this range measurements were carried out on our heterojunctions based on Cu(In,Ga)Se_2], an energy range of about 240 meV at room temperature and of about 120 meV at 150 K can be investigated during one frequency scan. In order to cover a broader energy range in the band gap, measurements at different temperatures have to be carried out. For an attempt-to-escape frequency $\nu_0=10^{11}$/s ($\nu_0=N_v\beta_p$), which is a typical value for Cu(In,Ga)Se_2 an energy depth from 80 to about 600 meV can be investigated for temperatures from 80 to 350 K. A limit of the energy range that can be investigated is imposed by the condition that only states deeper than the Fermi level in the bulk can be observed by this method.

In order to obtain the energy distribution of the defects, the capture cross section and therefore the attempt-to-escape frequency have to be known according to (20). For a discrete defect or a narrow maximum of the density of states distribution, this can be obtained by plotting the angular frequency at which the capacitance drops in (12) for different temperatures versus the inverse temperature (Arrhenius plot) and taking the intersect with the frequency axis. For a distribution of defects that does not exhibit any pronounced extrema, this method cannot be applied any longer. Then the attempt-to-escape frequency has to be fitted in such a way that the calculated defect distributions coincide in the overlapping energy ranges of measurements at different temperatures. This is illustrated in Fig. 8 where the defect distribution derived from calculated admittance data for a Gaussian defect as input at different temperatures is shown for the correct attempt-to-escape frequency, i.e., the input value, and under the assumption of an incorrect value for ν_0.

In general defect distributions are reproduced well by the method proposed above. Both the slope and the absolute values of tail-like distributions can be evaluated from admittance data. For Gaussian defect distributions a broadening of about 20 meV occurs with respect to the input data. The deviation for narrow distributions is certainly related to the violation of the condition that the distribution has to be constant within $\pm 2kT$. The absolute values depend on the assumed band profile of the junction and the related position dependence of the modulation signal. This is certainly a source for errors in an experiment as the exact band profiles are difficult to obtain. A more accurate correction factor can be obtained by calculating the band diagram with numerical codes (ADEPT[22]) and extracting the drop of the modulation signal from these data. A condition that is related to this problem is a uniform distribution of defects in space. A correct interpretation of an energy distribution of states requires a uniform distribution of defects in space due to the fact that defects at the intersect of the demarcation energy with the Fermi level are detected. Thus a shift of the demarcation energy by changing the angular frequency also results in a shift of the position in the junction where states are detected. Therefore, defects closer to the interface are interpreted as deeper in energy (for $p>n$ as explained above) which only gives a meaningful picture of the defect distribution in energy if this defect distribution is uniform in space. However, when applying a dc bias during the ac measurements, i.e., by varying the position in the junction at which the Fermi level intersects the defect level, nonuniform distributions of defects in space can be analyzed.

A source of misinterpretation results from the fact that admittance spectroscopy cannot distinguish between valence band and conduction band states. If valence and conduction band states are similar in shape and density, the analysis of admittance data would lead to an enhanced defect density of one type. Therefore, additional measurements such as DLTS are required in order to identify the nature of the defects. Another way to identify the nature of the defects measured by admittance spectroscopy consists of determining the $C(V)$ (capacitance–voltage) characteristics of a junction. By varying the applied dc bias the occupation of the defects changes and therefore their contribution to the space charge in the depletion region. As demonstrated by Kimerling,[23] the nature of the deep defects influences the slope of a Mott–Schottky plot [$1/C^2(V)$ vs V]. Thus it should be possible to determine the nature of defects by combination of $C(\omega)$ and $C(V)$ measurements.

Another problem is related to the question whether interface states (for example, at the heterointerface of a heterojunction) or defects in the bulk of the semiconductor are measured. Only defects at the position of the Fermi level at the interface can be charged and discharged and therefore contribute to the junction capacitance. However, if a broad distribution of defects is deduced from the measurements, these defects cannot be attributed to an interface where the Fermi level is fixed with respect to the bands. If a discrete defect level is deduced, bias dependent admittance measurements involving the change of the position of the Fermi level at the interface can be carried out. If a broad distribution of

defects exists at the interface, the measured energy depth should vary with the applied dc bias as the position of the Fermi level depends on the applied dc bias. These arguments should help to identify the nature of the measured defects.

V. APPLICATION TO ADMITTANCE MEASUREMENTS ON $CuInSe_2$ AND $Cu(In,Ga)Se_2$ THIN FILM SOLAR CELLS

$CuInSe_2$ and related materials can be used as the absorber layer in thin film solar cells, yielding efficiencies in excess of 17%.[24] Several studies were devoted to the study of states in the band gap of this material by DLTS,[25,26] PL,[27,28] admittance spectroscopy,[11,14] photoacoustic spectroscopy (PAS),[29] and thermally stimulated currents (TSCs).[30] Recently, modulated photocurrent (MPC) measurements provided evidence for the existence of a broad defect distribution in $CuIn(S,Se)_2$ thin films.[6] From these studies it can be expected that the electrical properties of the material itself as well as the performance of the corresponding solar cells depend to a large extent upon the properties of the gap states.[31] The procedure proposed for the evaluation of $C(\omega)$ was applied to measurements on a $CuInSe_2$ (CIS) and a $Cu(In,Ga)Se_2$ (CIGS) thin film solar cell.

A. Experiment

Polycrystalline $Cu(In,Ga)Se_2$ thin film solar cells with a total thickness of about 3 μm were prepared by coevaporation of Cu, In, Ga, and Se onto Mo-coated soda-lime glass substrates.[8] The window consisted of a chemical bath deposited CdS buffer layer and sputter deposited n-ZnO.[8] The resulting solar cell structure represents an n^+p heterojunction that can readily be used for admittance spectroscopy.

The cells investigated were a $CuInSe_2$ cell with $In/(In+Cu)=0.55$ (CIS) and a $Cu(In,Ga)Se_2$ (CIGS) cell with $Ga/(In+Ga)=0.15$, $(Ga+In)/(Ga+In+Cu)=0.54$ as determined by energy dispersive spectroscopy (EDS). The typical total area efficiency of these devices was between 11%–12%.

Four point admittance measurements were carried out at zero bias using a Hewlett Packard HP4192A impedance analyzer at frequencies ranging from 100 Hz to 1 MHz. The admittance data were evaluated assuming a parallel equivalent circuit. The amplitude of the ac signal was chosen between 20 and 50 mV. For the measurements the sample was mounted onto a LN_2-coolable sample stage inside a vacuum chamber, allowing the sample temperature to be varied between 80 and 400 K.

B. Admittance measurements

The frequency dependence of the device capacitance $C(f)$ and the contribution of traps to the device conductance G_t/ω for different temperatures are displayed in Figs. 9(a) and 9(b) for the CIS cell. Figures 10(a) and 10(b) show the corresponding data for the CIGS cell. To separate the contribution of traps to the conductance G_t, the dc conductance was subtracted from the measured values. However, inaccuracies in this procedure have a large impact at high frequencies as both graphs show: in Fig. 9(b) the trap conductance becomes negative for high frequencies while in Fig. 10(b)

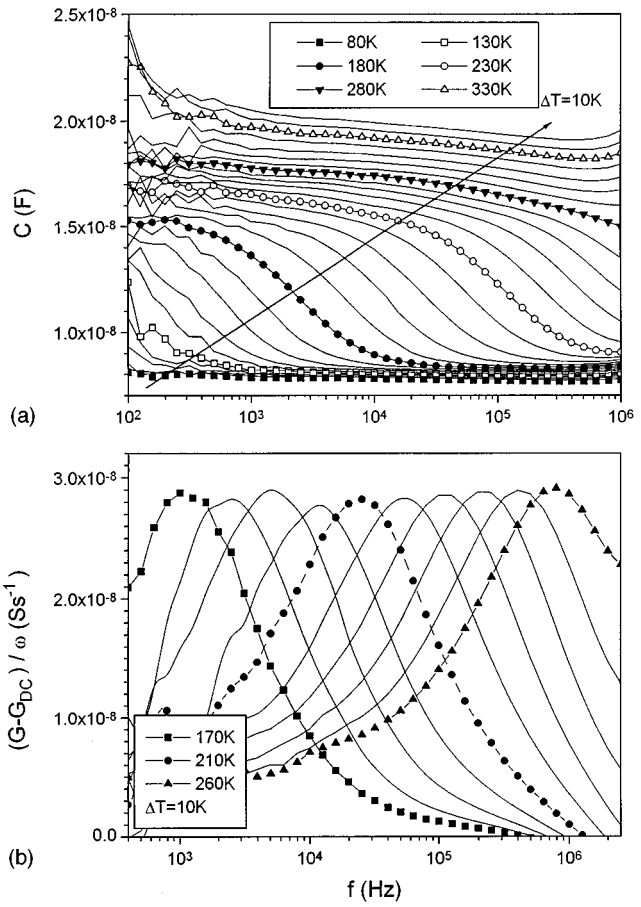

FIG. 9. Temperature dependent admittance measurements (10 K steps) on the $CuInSe_2$-based (CIS) heterojunction. (a) Frequency dependence of the capacitance, (b) frequency dependence of the trap contribution to the device conductance G_t/ω.

the curves are bent upward. It was mentioned above that the information contained in conductance and capacitance is equivalent. A discrete level produces a peak in G_t/ω at the position given by Eq. (20).[32] All the following results were derived from the $C(f)$ curves, as in this case the defect contribution is isolated by taking the derivative.

The $C(f)$ curves reveal that in both cases the device capacitance measured at room temperature is largely dominated by contributions from defect levels in the band gap. As expected, the features in the spectra shift to higher frequency with increasing temperature according to the temperature dependence of the detrapping time constants. The $C(f)$ spectra of the CIS cell [Fig. 9(a)] show a distinct step, whereas the dispersion in case of the CIGS cell appears to be rather continuous [Fig. 10(a)]. The effect of a resonance in the admittance begins to show as the frequency approaches 1 MHz.[33] Therefore only frequencies below 200 kHz were used to evaluate the defect distribution. In order to exclude interface states or spatial inhomogeneities as responsible for the observed frequency dispersion of the capacitance, admittance measurements depending on the applied dc bias were carried out (results are not shown). However, the transition frequency of the distinct step in Fig. 9(a) did not change with the applied dc bias (-2.5 to -0 V).

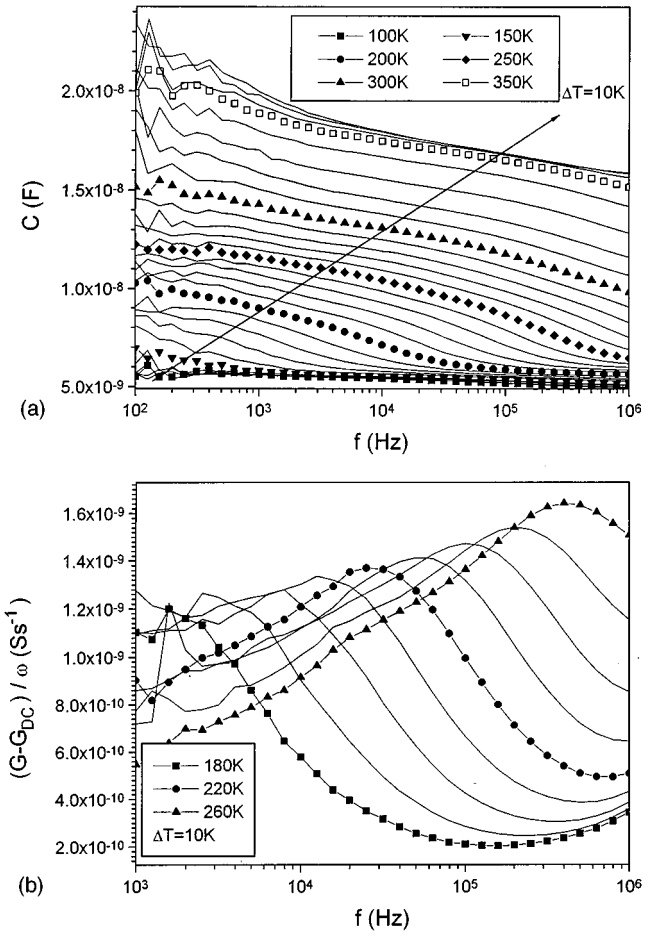

FIG. 10. Temperature dependent admittance measurements (10 K steps) on the $Cu(In,Ga)Se_2$ based (CIGS) heterojunction. (a) Frequency dependence of the capacitance, (b) frequency dependence of the trap contribution to the device conductance G_t/ω.

The attempt-to-escape frequency $\nu_0=\beta_p N_v$ for the states in a maximum of the density of states can be obtained from an Arrhenius plot of the maxima of $\omega \cdot dC/d\omega$ vs ω (Fig. 11). The temperature dependence $\nu_0 \sim T^2$, arising from the temperature dependencies of the thermal velocity v_{th} contained in the capture coefficient and N_v, does not affect the results of the analysis and was therefore neglected.

For the CIS cell an attempt-to-escape frequency of $\nu_0=6.2\times10^{11}\ \mathrm{s}^{-1}$ and an activation energy of 280 meV were deduced. For the CIGS cell $\nu_0=1.1\times10^{12}\ \mathrm{s}^{-1}$ and an activation energy of 310 meV were found.

Starting from the above values of the attempt to escape frequency, the defect distribution was calculated from (25) for linear bands. Using the parabolic band model, that would be in principle more appropriate for our n^+p junctions, requires *a priori* knowledge as to whether the defects represent hole or electron traps. For the effective density of states in the valence band at room temperature $N_v=10^{19}\ \mathrm{cm}^{-3}$ was used according to the effective masses given by Neumann for $CuInSe_2$.[34]

To obtain the density of states, the measurements between 1 and 200 kHz were used. As the derivative of $C(f)$ has to be taken, the low frequencies had to be disregarded because of the noise in the spectra. The high frequencies

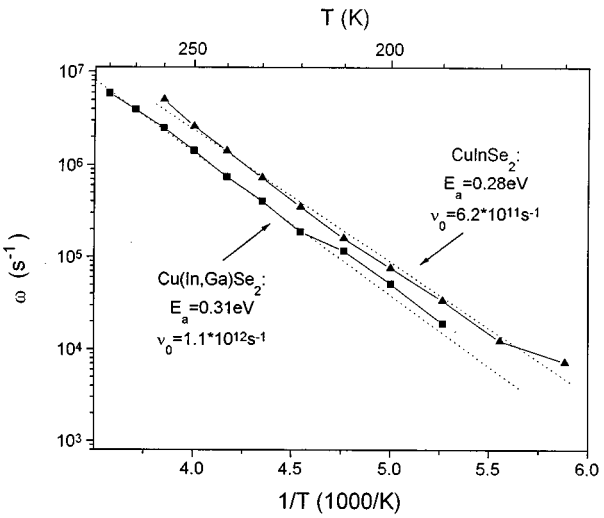

FIG. 11. Arrhenius plots of the angular frequencies of the maxima of $\omega \cdot dC/d\omega$.

were not used due to the resonance mentioned above. The resulting densities of states are shown in Fig. 12 and Fig. 13 for the CIS and for the CIGS cells, respectively. Estimate values for the carrier density, used to obtain the built-in voltage U_d and the space charge width w, were taken from $C(V)$ measurements and are given in Figs. 12 and 13. The presence of a large density of deep traps makes it difficult to obtain the carrier density from $C(V)$ measurements, even if a test frequency is chosen, at which the ac occupation of the deep centers cannot follow.[23] A discussion of $C(V)$ measurements is not within the scope of the present article but will be published later. The resulting error in the determination of the built-in voltage and the space charge width is expected to be within $\pm 25\%$ for both devices. The main errors introduced in the absolute values of the density of states of Fig. 12 and Fig. 13 are most likely due to the assumption of linear bands. These limitations have to be kept in mind when judging the absolute values of the defect densities.

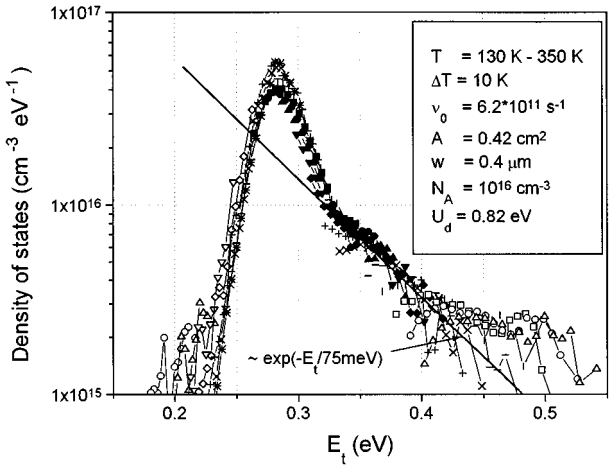

FIG. 12. Defect distribution of the $CuInSe_2$-based (CIS) heterojunction.

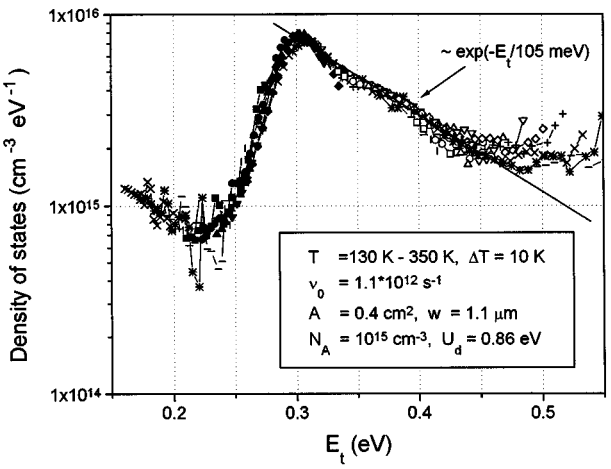

FIG. 13. Defect distribution of the Cu(In,Ga)Se_2-based (CIGS) heterojunction.

At each temperature a frequency scan yields information on a part of the band gap depending on the attempt-to-escape frequency. For both cells the individual defect densities deduced from measurements at different temperatures are in good agreement. Adjacent to the maximum of the density of states detected by the admittance measurements at 280 and 310 meV for the CIS and CIGS cells, respectively, a tail-like defect distribution extends towards midgap similar to the results of previous MPC investigations.[6] The characteristic energies of this defect distribution are about 75 meV for the CIS cell and 105 meV for the CIGS cell. These values are in agreement with the diode ideality factors of solar cell devices, assuming that recombination takes place via a tail-like defect distribution.[31] The pronounced step in the $C(f)$ curves of the CIS device [Fig. 9(a)] corresponds to the defect peak at 280 meV (Fig. 12) whereas the $C(f)$ curves of the CIGS device [Fig. 10(a)] are dominated by a continuous dispersion that is reflected in a broader defect distribution (Fig. 13). The decrease of the defect density towards the band edge might also be due to the position of the Fermi level in the bulk of the p-type absorber layer, limiting the range in which defects in the lower part of the band gap may be detected. Careful comparison of the density of states of the CIS cell between 400 and 500 meV suggests a shift among the curves for different temperatures, pointing to a higher attempt-to-escape frequency for the corresponding states as compared to the peak at 280 meV. As illustrated in Fig. 2(d), the density of states estimated from $C(f)$ is expected to approach zero towards midgap since due to recombination the midgap states are not accessible unless the capture coefficient for holes and electrons differs greatly, thus providing another indication of a higher capture coefficient close to midgap.

The similarity of these results to the defect distribution found in MPC measurements[6] and a prominent 250–260 meV hole trap found in DLTS investigations[25] suggests that the density of states observed here is situated in the lower half of the band gap. Due to the width of the defect distribution they clearly do not represent the interface states explained above.

The high density of gap states as compared to the estimated carrier concentration shows the impact that these states will have on the electrical properties.

VI. CONCLUSIONS

A method that allows the determination of defect levels distributed in energy from zero bias junction admittance measurements was proposed. This procedure reproduces the defect distribution with sufficiently high accuracy. The limitations of this method were discussed and measurement techniques to obtain additional information were proposed.

The application to heterojunctions of p-Cu(In,Ga)Se_2 thin films with n-ZnO revealed a broad defect distribution that agreed well with previously published results.

[1] D. V. Lang, J. Appl. Phys. **45**, 3023 (1974).
[2] H. Oheda, J. Appl. Phys. **52**, 6693 (1981).
[3] R. Rose, *Concepts in Photoconductivity* (Interscience, New York, 1963).
[4] P. G. LeComber and W. E. Spear, Phys. Rev. Lett. **25**, 509 (1970).
[5] D. V. Lang, Phys. Rev. **25**, 5330 (1982).
[6] R. Herberholz, T. Walter, and H. W. Schock, J. Appl. Phys. **76**, 2909 (1994).
[7] Y. Tang, R. Braunstein, and B. von Roedern, Appl. Phys. Lett. **63**, 2393 (1994).
[8] W. Bloss, F. Pfisterer, M. Schubert, and T. Walter, Prog. Photovolt. **3**, 3 (1995).
[9] J. Werner and W. Peisl, Phys. Rev. B **31**, 6881 (1985).
[10] D. L. Losee, J. Appl. Phys. **46**, 2204 (1975).
[11] J. Santamaria, G. Gonzalez Diaz, E. Iborra, I. Martil, and F. Sanchez-Quesada, J. Appl. Phys. **65**, 3236 (1989).
[12] M. Beguwala and C. R. Crowell, Solid-State Electron. **17**, 203 (1974).
[13] C. Tan and M. Xu, Solid-State Electron. **32**, 25 (1989).
[14] M. Schmitt, U. Rau, and J. Parisi, 13th European Photovoltaic Solar Energy Conference, Nice, France, 1995.
[15] J. L. Pautrat, B. Katircioglu, N. Magnea, D. Bensahel, J. C. Pfister, and L. Revoil, Solid-State Electron. **23**, 1159 (1980).
[16] G. I. Roberts and C. R. Crowell, J. Appl. Phys. **41**, 1767 (1970).
[17] C. Barret, F. Chekit, and A. Vapaille, J. Phys. C **16**, 2421 (1983).
[18] D. Caputo, G. de Cesare, U. Forghieri, F. Irrera, G. Masini, F. Palma, and M. Tucci, in Ref. 14.
[19] D. Maier, P. Hug, M. Fiederle, C. Eiche, D. Ebling, and J. Weese, J. Appl. Phys. **77**, 3851 (1995).
[20] I. Balberg and E. Gal, J. Appl. Phys. **58**, 2617 (1985).
[21] I. Balberg, J. Appl. Phys. **58**, 2603 (1985).
[22] J. Gray, IEEE Trans. Electron Devices **36**, 906 (1989).
[23] L. C. Kimerling, J. Appl. Phys. **45**, 1839 (1974).
[24] M. A. Contreras, J. Tuttle, A. Gabor, A. Tennant, K. Ramanathan, S. Asher, A. Franz, J. Kaine, L. Wang, J. Scofield, and R. Noufi, Proceedings of the 1st World Conference on Photovoltaic Energy Conversion, Hawaii, 1994, p. 68.
[25] M. Igalson and R. Bacewicz, Proceedings of the 11th European Photovoltaic Solar Energy Conference, Montreux, Switzerland, 1992, p. 874.
[26] A. L. Li and I. Shih, J. Electron. Mater. **22**, 195 (1993).
[27] F. A. Abou Elfotouh, L. L. Kazmerski, H. R. Moutinho, J. M. Wissel, R. G. Dhere, A. J. Nelson, and A. M. Bakry, J. Vac. Sci. Technol. **9**, 554 (1991).
[28] M. Tanda, S. Manaka, J. R. Encinasmarin, K. Kushiya, H. Sano, A. Yamada, M. Konagai, and K. Takahashi, Jpn. J. Appl. Phys. **31**, L753 (1992).
[29] A. Zegadi, D. M. Bagnall, M. A. Slifkin, H. Neumann, and R. D. Tomlinson, Proceedings of the 12th European Photovoltaic Solar Energy Conference, Amsterdam, 1994, p. 1576.
[30] T. Datta, R. Noufi, and S. K. Deb, J. Appl. Phys. **59**, 1548 (1986).
[31] T. Walter, R. Menner, Ch. Köble, and H. W. Schock, in Ref. 29, p. 1755.
[32] S. R. Dhariwal and B. M. Deoraj, Solid-State Electron. **36**, 1165 (1993).
[33] J. H. Scofield, Sol. Cells **37**, 217 (1995).
[34] H. Neumann, Sol. Cells **16**, 317 (1986).